Cancer Letters 466 (2019) 1–12

Contents lists available at ScienceDirect

Cancer Letters

journal homepage: www.elsevier.com/locate/canlet

Original Articles

Glioblastoma extracellular vesicles induce the tumour-promoting transformation of neural stem cells

Jian Wang[a,b,1], Jialin Liu[a,1], Guochen Sun[a,1], Hengxing Meng[a], Jiayin Wang[c], Yunqian Guan[d], Yiheng Yin[a], Zhenyu Zhao[a], Xiying Dong[a], Shangjiong Yin[b], Hongwei Li[e], Yuefei Cheng[b], Hao Wu[a], Anhua Wu[f,**], Xinguang Yu[a,***], Ling Chen[a,*]

[a] Department of Neurosurgery, Chinese People's Liberation Army of China (PLA) General Hospital, Medical School of Chinese PLA, Institute of Neurosurgery of Chinese PLA, Beijing, 100853, China
[b] Department of Neurosurgery, Hospital of Eighty-first Army Group of Chinese PLA, Zhang Jiakou, 075000, China
[c] Department of Medicine, Surgery, and Cell Biology, The University of Oklahoma Health Sciences Center, Stanton L. Young Biomedical Research Center, Oklahoma City, OK, 73104, USA
[d] Department of Cell Biology, Xuanwu Hospital, Capital Medical University, Beijing, 100053, China
[e] Department of Pathology, Hospital of Eighty-first Army Group of Chinese PLA, Zhang Jiakou, 075000, China
[f] Department of Neurosurgery, The First Hospital of China Medical University, Shenyang, 110122, China

ARTICLE INFO

Keywords:
Glioblastoma
Neural stem cells
Extracellular vesicles
Single cell sequencing

ABSTRACT

Recurrent glioblastomas are frequently found near subventricular zone (SVZ) areas of the brain where neural stem cells (NSCs) reside, and glioblastoma-derived extracellular vesicles (EVs) are reported to play important roles in tumour micro-environment, but the details are not clear. Here, we investigated the possibility that NSCs are involved in glioblastoma relapse mediated by glioblastoma-derived EVs. We studied changes to NSCs by adding glioblastoma-derived EVs into a culture system of NSCs, and found that NSCs differentiated into a type of tumour-promoting cell. These transformed cells had distinguished proliferation activity, a high migration rate, and clone-forming ability revealed by CCK-8, wound healing and soft agar clone formation assays, respectively. In vivo assays indicated that these cells could accelerate tumour formation by Ln229 cells in nude mice. Moreover, to explore the mechanisms underlying NSC transformation, single cell transcriptome sequencing was performed; our results suggest that several key genes such as *S100B*, *CXCL14*, *EFEMP1*, *SCRG1*, *GLIPR1*, *HMGA1* and *CD44* and dysregulated signalling may be important for the transformation of NSCs. It is also indicated that NSCs may be involved in glioblastoma recurrence through EV release by glioblastoma in this work. This could help to illuminate the mechanism of glioblastoma relapse, which occurs in a brief period after surgical excision, and contribute to finding new ways to treat this disease.

1. Introduction

Glioblastoma is one of the most common and aggressive cancers found in central nervous system and has been classified as a Grade IV astrocytic tumour with poor prognosis based on the WHO classification [1]. Although the median life expectancy and 2-year survival rate for glioblastoma patients have been improving [2], the 5-year overall survival rate is still only 9.8%, even after combined treatments of

Abbreviations: CM, conditioned media; CSC, cancer stem cell; EGFR, epidermal growth factor receptor; EV, extracellular vesicle; GAPDH, glyceraldehyde phosphate dehydrogenase; GFAP, glial fibrillary acidic protein; MOG, myelin oligodendrocyte glycoprotein; NSC, neural stem cell; PPAR, peroxisome proliferator-activated receptor; Sox2, sry related HMG box-2; SVZ, subventricular zone; TEM, transmission electron microscopy; WGCNA, weighted gene co-expression network analysis

* Corresponding author. Department of Neurosurgery, Chinese People's Liberation Army of China(PLA) General Hospital, Medical School of Chinese PLA, Institute of Neurosurgery of Chinese PLA, 28 Fuxing Road, Haidian District, Beijing, 100853, China.
** Corresponding author. Department of Neruosurgery, The First Hospital of China Medical University, 155 Nanjing Road, Heping District, Shenyang, 110122, China.
*** Corresponding author. Department of Neurosurgery, Chinese People's Liberation Army of China (PLA) General Hospital, Medical School of Chinese PLA, Institute of Neurosurgery of Chinese PLA, 28 Fuxing Road, Haidian District, Beijing, 100853, China.
E-mail addresses: wuanhua@yahoo.com (A. Wu), xinguang_yu@263.net (X. Yu), chen_ling301@163.com (L. Chen).
[1] Co-first authors: Jian Wang, Jialin Liu, and Guochen Sun.

https://doi.org/10.1016/j.canlet.2019.09.004
Received 30 May 2019; Received in revised form 6 September 2019; Accepted 9 September 2019

concomitant adjuvant temozolomide and radiotherapy [3]. Neural stem cells (NSCs) often reside in the subventricular zone (SVZ) of the adult mammalian brain [4]; similarly, glioblastomas are frequently found to originate from the same areas or nearby regions [5]. Researchers have also discovered that many neural precursor cells migrate towards brain tumours like glioblastomas [6], and thus, it is important to clarify whether NSCs are involved in glioblastoma relapse.

Extracellular vesicles (EVs) including exosomes and micro-vesicles are small vesicles secreted by almost all cells in the human body. There has been a surge in literature that accentuates the unique role that EVs play in mediating communications between cells [7–9]. Specifically, they have been found in many tumours and are thought to be involved in tumour angiogenesis [10], invasion [7], metastasis [9], recurrence, and related drug resistance [11]. In glioblastomas, EVs participate in the biogenesis of glioma, the modification of its micro-environment, and disease progression; they could also be used as tumour biomarkers for diagnosis and prognosis or as potential therapeutic targets/delivery systems [12–18].

In this study, we show that EVs derived from glioblastoma alter the phenotype and biological behaviours of NSCs in vitro, and that tumour formation by Ln229 cells was enhanced by these transformed cells in vivo. To investigate the potential mechanism underlying this process, a single-cell transcriptome analysis, first applied in 2009 [19], was performed. With this high-throughput technology, it is feasible to profile thousands of cells simultaneously, and unbiased insights into the heterogeneity of single cells within the transformed population have been obtained [20,21]. Here, different clusters within the transformed cells were identified, a key group of differentially expressed genes was also unveiled and analysed, and we found that dysregulated signalling took place during this “stem to tumour-promoting” cell transformation.

2. Materials and methods

2.1. Cell culture

All studies were carried out in accordance with the Declaration of Helsinki developed by The World Medical Association. All experiments were approved by the ethic committee of Chinese PLA General Hospital. The glioblastoma T0 cell line was established from a patient with recurrent glioblastoma (male). The WJ02 cell line was established from a patient (male) with a seizure disorder during an epilepsy-focused resection. Both patients signed the complete informed consent forms before their operations. The samples were minced and digested in a digesting buffer (papain solution, 2 mg/ml; L-cysteine, 0.36 mg/ml; DNAseI, 50 μg/ml; Sigma) at 37 °C for 20 min, and later filtered with 40-μm strainers (FALCON). The mixtures were then separated at 300 × *g* for 5 min using a centrifuge (Thermo Scientific). After discarding the supernatant, cells were suspended with Dulbecco's modified Eagle's medium (DMEM, Corning) supplemented with a 10% foetal bovine serum (FBS, MOREGATE), and the cells were maintained at 37 °C in a 5% CO_2 incubator (Thermo Scientific).

The Ln229 cell line (glioblastoma, gifted by the Neurosurgery Department of Tianjin General Hospital, Tianjin, China) was cultured in DMEM supplemented with 10% FBS at 37 °C in a 5% CO_2 incubator.

Neural stem cells [22] (NSCs, derived from a human embryo, 3 months of age, male; gifted by the Department of Cell Biology of Xuanwu Hospital, Beijing, China) were cultured in NSC-medium comprised of neurobasal medium (Gibco, Life Tech) supplemented with B27 (20 μl/ml, Life Tech), recombinant human epidermal growth factor (Hu EGF, 20 ng/ml; Life Tech), recombinant human fibroblast growth factor-basic (FGFb, 20 ng/ml; Life Tech), penicillin streptomycin solution (penicillin, 100 U/ml; streptomycin, 100 μg/ml; Corning) and GlutaMAX (10 μl/ml; Life Tech), at 37 °C in a 5% CO_2 incubator.

The culture medium of the glioblastoma cell line or WJ02 cells was discarded when glioblastoma cells grew to 80% confluency, which was followed by three washes with a sterile phosphate buffered saline (PBS) solution. Then, FBS-free DMEM was used for culture; after another 48 h, the conditioned media (CM) was collected, centrifuged at 1000 × *g* for 20 min to remove the debris, and filtered with a 40-μm strainer. Then, the media were stored at 4 °C or used as described.

NSCs were then maintained in NSC-medium with the addition of EVs extracted from CM of Ln229 cells every 2 days at 37 °C in a 5% CO_2 incubator for 6 weeks (EV concentration was 10 μg/ml). The resulting cells were named NSC-Ln229ev cells.

2.2. Animals

All mouse work was performed in accordance with institutional, IACUC, and AAALAS guidelines, under the animal protocol 0709-666A. All animal studies were conducted following approval from the Animal Care and Use Committee of Chinese PLA General Hospital. Six-week-old BALB/c male nude mice (Beijing Vital River Laboratory Animal Tech) were raised in pathogen-free devices, with sterile food and water supplied. Ln229 cells (2×10^6) alone or together with NSC-Ln229ev cells (at a 4:1 cell ratio, 1.6×10^6 Ln229 cells to 4×10^5 NSC-Ln229ev cells) were suspended in 200 μl serum-free DMEM and then transplanted into either the left or right flank of each mouse. Tumour formation was monitored for 8 weeks, and then the mice were sacrificed. The tumours were then excised, measured, and photographed. Immunohistochemistry was performed to detect the presence of related markers.

2.3. EV extraction

CM derived from Ln229 or WJ02 cells was treated as described previously herein, followed by concentration with a centrifugal filter (100 K, Millipore) at 4500 × *g* for 20 min using a centrifuge. EVs were then extracted from the concentrated CM with the exo-Easy Maxi Kit (QIAGEN, Hilden, Germany) according to the manufacturer's protocol. The residual liquid derived from CM was named R-CM, and used for a control group.

2.4. Transmission electron microscopy (TEM)

The freshly extracted EVs were fixed with 2% glutaraldehyde (Sigma) and stored at 4 °C overnight. The mixture was then treated with 1% osmium tetroxide (Sigma), contrasted with 4% uranyl acetate (Sigma) for 2 min and picked up on copper thin bar 200-mesh grids, and dehydrated with 100% ethanol. Samples were examined with a transmission electron microscope (HT7700, Hitachi, Japan) at 80.0 kV.

2.5. EV particle size analysis

The freshly extracted EVs were prepared in PBS solution and added to a disposable sample pool. The sample pool was examined by a ZETASIZER Nano series-Nano-ZS (Malvern), and a total of five 60-s frames was collected per trial using NTA software (Malvern) with auto-detectable settings. The data from the five collections were averaged for the distributional analysis of EVs in each trial.

2.6. EV surface marker analysis

The freshly-extracted EVs were washed with PBS solution once and then incubated with anti-CD63-FITC (BD) and anti-CD81-FITC (BD) antibodies separately in different containers at room temperature for 30 min. One set of EVs were also incubated with PBS as a control group. All samples were washed three times with PBS solution; then, samples were detected with an Accuri C6 flow cytometer (BD).

2.7. Cell proliferation assay

The proliferation curves of cells were measured using Cell Counting

Kit-8 (CCK-8, Dojido) according to the manufacturer's protocol. Proliferation curves were produced using GraphPad Prism 5.

2.8. Soft agar clone formation assay

Approximately 1000 cells were plated in 1 ml of culture medium containing 0.3% (w/v) agar (Invitrogen) over a 1 ml solid plug of culture medium with 0.7% (w/v) agar as the gelling agent in a 12-well plate. Four weeks later, all formed clones in each well were photographed with a digital camera (Nikon D7200), and counted under a phase-contrast microscope (Nikon Eclipse TS100).

2.9. Invasion assay

NSC-Ln229ev cell clones formed during the soft agar clone formation assay were maintained for another 12 weeks with the culture media continuously replaced once per week. Digital camera images of the clones were captured at the 8th and 16th week. The diameters of clones at each time point were measured by Image J Software and compared.

2.10. Wound-healing assay

Cells were harvested in 1 ml of culture media and plated into 6-well plates, reaching 100% confluency within 24 h. Each type of cell was then plated in six-well dishes, and scratch lines were made with 200-μl pipette tips. The culture medium was then replaced with FBS-free DMEM medium, and cells were cultured for another 24 h. Digital camera images were captured at 0 h and 24 h under a phase-contrast microscope. Wound-healing areas for each type of cell were measured using Image J software.

2.11. Transwell assay

Approximately 2×10^4 cells were plated into Cell Culture Inserts (8 μm, 24-well Hanging inserts, Millipore) coated with Matrigel (Corning, 300 μg/ml, 37 °C, 2 h), with the addition of 250 μl FBS-free DMEM; 750 μl culture medium supplemented with 10% FBS was added to in the bottom chamber. Cells were maintained for 24 h at 37 °C in a 5% CO_2 incubator. Next, cells on the upper surface of inserts were scraped away, and migrated cells on the lower surface were fixed and stained with 0.05% crystal violet (Sigma) for 2 h at 37 °C. Images under a phase-contrast microscope were captured with a digital camera.

2.12. Single-cell sequencing and data analysis

Cells were harvested and filtered with 40-μm strainers to form single-cell suspensions. The single-cell RNA-seq libraries were generated with the Chromium Single Cell 3′ Reagent Kit (10 × Genomics), and the single-cell suspensions and real-time polymerase chain reaction (RT-PCR) Master Mix were loaded together with Single Cell 3′ Gel Beads and Partitioning Oil into a Single Cell 3′ chip (10 × Genomics) according to the manufacturer's protocol. RNA transcripts from single cells were barcoded and reverse-transcribed within droplets, which was followed by the construction of complementary DNA (cDNA) libraries of single cells according to the manufacturer's protocol. All libraries were quantified by Agilent2100 and real time quantitative PCR on an ABI 7500 system (Life Tech). All single-cell libraries were sequenced on an Illumina Novaseq system (Illumina), and the data was aligned and quantified with Cell Ranger Single-Cell Software (10 × Genomics, version 2.0.2). The processed data were then loaded into Seurat software for normalization, dimensionality reduction (t-distributed Stochastic Neighbour Embedding, t-SNE), and downstream analysis. The expression data from each cell were normalized to the sequencing depth of 10,000 reads and log-transformed. After normalization, the highly variable genes were identified using the Seurat FindVariableGenes function. The cell clusters were identified using the FindClusters algorithm and marker genes in each cluster were identified using the FindAllMarkers function in Seurat with default parameters. To identify the enriched pathways for genes in each cluster, KEGG pathway analysis was performed using the R KEGGprofile package (version 1.22.0).

2.13. Western blotting

Proteins (30 μg) from EVs and whole cell lysates were loaded on NuPAGE 4–12% Bis-Tris Gel (Novex, Life Tech), which was followed by electrophoresis using a Mini Gel Tank (Life Tech), and were then transferred onto 0.45-μm polyvinylidene fluoride (Millipore) membranes using a Mini Blot Module (Life Tech). The membranes were blocked with 5% milk for 1 h at room temperature. After primary antibodies were added, the membranes were incubated at 4 °C overnight. The primary antibodies used were anti-CD9 (1:1000; Abcam ab92726), anti-glyceraldehyde phosphate dehydrogenase (GAPDH, 1:1000; Beyotime AG019), anti-glial fibrillary acidic protein (GFAP, 1:1000; Abcam ab68428), and anti-sry related HMG box-2 (Sox-2, 1:1000; Abcam ab92494). After three washes, the membranes were incubated with the appropriate HRP-conjugated secondary antibodies (1:1000; Beyotime A0208) at room temperature for 1 h. The membranes were subjected to protein detection with a Chemiluminescence Kit (BeyoECL Star, Beyotime) after another wash, and the blots were photographed with a digital camera.

2.14. Immunocytochemistry

Cells were harvested and plated into 24-well plates on a cell culture slide, which was left overnight. Then, cells were fixed with 4% paraformaldehyde (Sigma) at room temperature for 10 min, followed by incubation with primary antibodies at 4 °C overnight. The primary antibodies used were as follows: anti-CD133 (1:200; Abcam ab222782), anti-Sox2 (1:200; Abcam ab92494), anti-Nestin (1:200; Abcam ab176571), anti-GFAP (1:200; Abcam ab68428), anti-CD68 (1:200; Abcam ab213363), anti-NeuN (1:200; Abcam ab177487), and anti-myelin oligodendrocyte glycoprotein (MOG, 1:200; Abcam ab109746). After three washes, the slides were incubated with Alexa 488-conjugated secondary antibodies (1:1000; Abcam ab150077) for 1 h at room temperature; then, another three washes were performed, followed by incubation with 300 μl DAPI solution (10 μg/ml, Beyotime) for 10 min. Fluorescence microscope (Leica DM5000B) images of the slides were captured using LAS AF software after three extra PBS washes.

2.15. Immunohistochemistry

Experimental animals were sacrificed after cells had been implanted for 8 weeks; formed tumours were resected, fixed in 10% neutral buffered formalin for 24 h, and later embedded in paraffin wax. Haematoxylin-eosin (HE) staining and immunohistochemistry were performed on 4-μm-thick serial sections. The sections were treated with an automatic immunohistochemical device (Roche Benchmark GX) according to the manufacturer's instructions. The primary antibodies used included anti-GFAP (1:200; MXB Kit-0031), anti-Nestin (1:200; Abcam ab176571), anti-Sox2 (1:200; Abcam ab92494), anti-S100 (1:200; MXB Kit-0007), anti-vimentin (1:200; MXB Kit-0019), and anti-Ki67 (1:200; MXB Kit-0005). The sections were photographed under a microscope.

2.16. Statistical analysis

Independent experiments were performed in triplicate for all studies except for single cell sequencing (performed once). Error bars from graphical data represent mean ± standard deviation (SD). Two-tailed

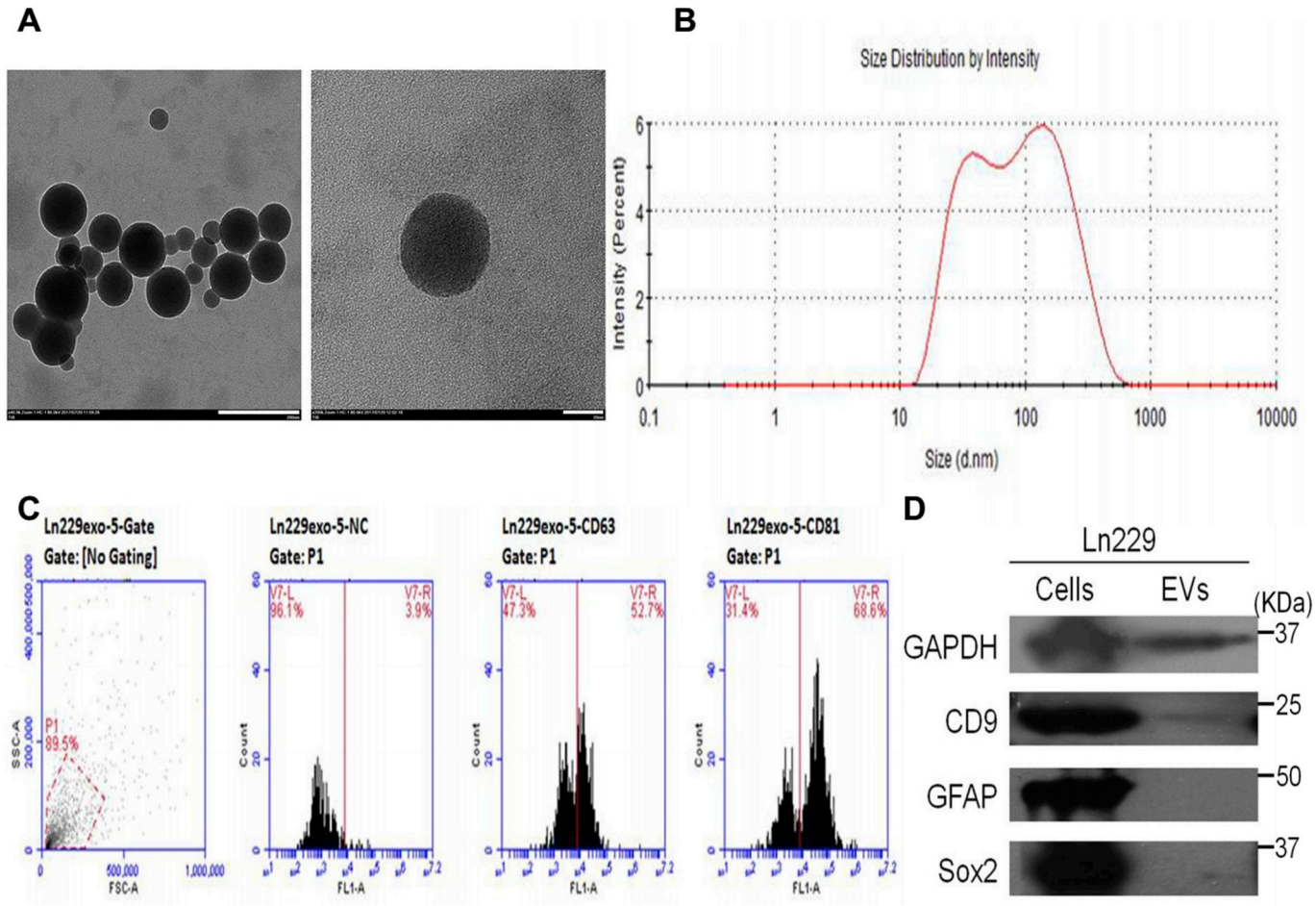

Fig. 1. Identification of EVs derived from Ln229 cells. (A) TEM images of extracted EVs from Ln229 cells. Magnification 40.0 K × . Scale bar, 200 nm (left). Magnification 200.0 K × . Scale bar, 20 nm (right). (B) Particle size analysis showed the size distribution of EVs from Ln229 cells. (C) Surface marker analysis of EVs from Ln229 cells, with CD63 and CD81 positively expressed. (D) Western blotting analysis of CD9, GAPDH, GFAP, and Sox2 in cell lysates and EVs. Proteins (30 μg) from EVs or whole cell lysates were loaded. Sox2 and GFAP were negative controls.

Student's *t*-tests were performed, and a *P*-value less than 0.05 was considered statistically significant. Statistical analyses were performed with SPSS 19.0 software.

3. Results

3.1. Identification of EVs extracted from the culture medium of glioblastoma cells

With an exo-Easy Maxi kit, a considerable quantity of EVs were harvested and the TEM results revealed their successful extraction (Fig. 1A). The particle sizes and their relevant distributions were analysed by a ZETASIZER Nano series-Nano-ZS; average sizes ranged from 55 to 99 nm, and the distribution is shown in Fig. 1B. Surface markers of EVs were identified by flow cytometry, and CD63 and CD81 were positively expressed in EVs derived from glioblastoma cells (Fig. 1C). Other EV markers such as CD9 and GAPDH were also detected by western-blotting (Fig. 1D).

3.2. Differentiation of NSCs induced by EVs from Ln229 cells

The EVs and CM derived from Ln229 cells were then respectively added to the culture medium of NSCs. After 6 weeks, a majority of the NSC spheres in these two groups adhered to the agar surface of flasks and differentiated into spindle cells. Those spindle cells migrated towards surrounding areas, adhering to one another by cellular processes, as shown in Fig. 2A (A–F), whereas this did not occur in control groups (Fig. 2A, G–R). The differentiated spindle cells were named either NSC-Ln229ev or NSC-Ln229CM based on whether EVs or CM from Ln229 cells were added. Neural cell markers were examined both before and after the addition of EVs into the culture medium. Expression of NSC markers like CD133, Sox2, and Nestin [23] was positive (Fig. 2B), whereas that of differentiated cell markers such as GFAP, CD68, NeuN, and MOG [23] was negative (see Supplementary Information Fig. S1) prior to EV addition. After the differentiation of NSCs into spindle cells upon the addition of EVs, CD133 expression was negative, with Sox2 and Nestin expression remaining positive (Fig. 2C). GFAP and NeuN expression was positive, while CD68 and MOG expression was still negative in NSC-Ln229ev cells (Fig. 2D).

3.3. Malignant capacity of NSC-Ln229ev cells

The proliferative activity of NSC-Ln229ev cells was assessed using a CCK-8 Kit. Differentiated cells proliferated more rapidly than NSCs, whereas the proliferation rates of NSC-Ln229ev and Ln229 cells were similar (Fig. 3A). Based on Ki67 expression assays, the positive expression rate of Ki67 in spindle cells was higher compared to that in NSCs (Fig. 3B), and the difference was statistically significant ($P < 0.001$, Fig. 3C). Regarding soft agar assays, clones formed by NSC-Ln229ev cells were observed (Fig. 3D), but there were no clones formed by NSCs (Fig. 3D and E).

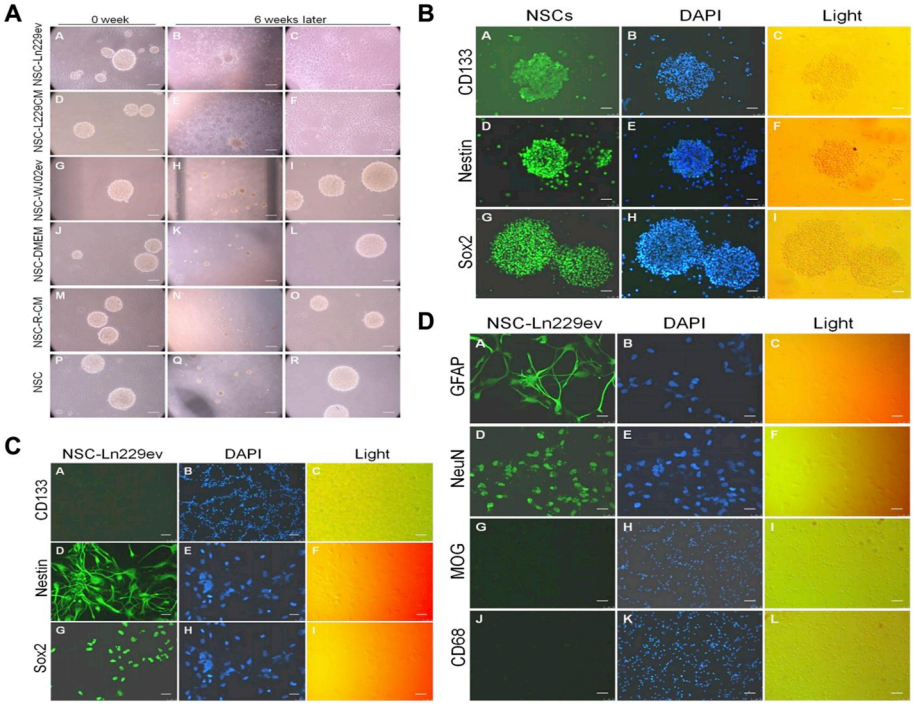

Fig. 2. Induction of NSCs by EVs derived from glioblastoma cells. (A) NSCs differentiated in the presence of EVs or CM derived from GBM cells (A–F), whereas in four control groups, NSCs showed no changes after 6 weeks (G–R). D-F, NSCs were cultured in a mixture medium, the proportion of NSC-medium to CM was 1:1. G-I, NSCs were maintained in the NSC-medium with addition of EVs from WJ02 cells (normal astrocytes), EVs concentration was 10 μg/ml. J-L, NSCs were cultured in the NSC-medium supplemented with an equal volum of FBS-free DMEM. M − O, NSCs were cultured in the NSC-medium supplemented with an equal volum of R-CM, R-CM was the residual liquid of CM, from which EVs had been extracted. P-R, NSCs were maintained in the NSC-medium with nothing else added. Magnification 20×, Scale bars, 10 μm (A,C,D,F,G,I,J,L,M,O,P,R). Magnification 4×, Scale bars, 50 μm (B,E,H,K,N,Q). (B) Stem cell markers were positively expressed in NSCs including CD133, Nestin, and Sox2. Magnification 20×, Scale bars, 50 μm (A–I). Nuclei were stained with DAPI. (C) CD133 showed negetively expressed in NSC-Ln229ev cells (A–C), while Nestin and Sox2 were still positive (D–I), Magnification 10×, Scale bars, 100 μm (A–C). Magnification 40×, Scale bars, 25 μm (D–I). Nuclei were stained with DAPI. (D) NSC-Ln229ev cells showed different expression patterns, with positively expressed GFAP and NeuN (A–F), and negatively expressed MOG and CD68 (G–L). Magnification 40×, Scale bars, 25 μm (A–F). Magnification 10×, Scale bars, 100 μm (G–L). Nuclei were stained with DAPI.

3.4. Migration and invasion ability of NSC-Ln229ev cells

To assess the migration and invasion ability of NSC-Ln229ev cells, several assays were performed. Results of wound-healing assays showed that NSC-Ln229ev cells migrated towards the wound areas as quickly as Ln229 cells (Fig. 4A), and there were no significant differences in recovery rates between the two groups (Fig. 4B, $P > 0.05$). The clones formed by soft agar assays were cultured for another 12 weeks, and the expansion of NSC-Ln229ev cells towards surrounding areas was obvious (Fig. 4C), with clones of Ln229 cells serving as the positive control. The invaded areas of NSC-Ln229ev cell clones at the 8th and the 16th week were measured and compared, and the difference was statistically significant (Fig. 4D, $P < 0.01$). Moreover, transwell assays were performed, and many NSC-Ln229ev cells successfully moved across the Matrigel-treated membrane after 24 h of culture in the upper chamber (Fig. 4E). In contrast, very few NSCs passed through the membrane (Fig. 4F, $P < 0.01$).

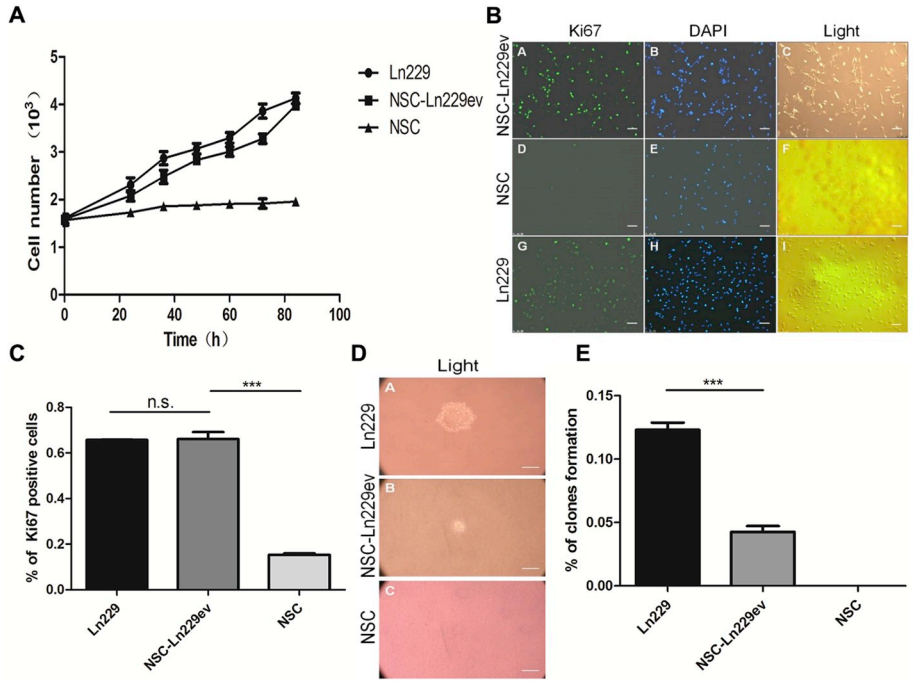

Fig. 3. Proliferation and clone formation of NSC-Ln229ev cells. (A) The proliferation curve showed that there were no significant differences between Ln229 and NSC-Ln229ev cells in proliferation rates ($P > 0.05$), whereas the differences between NSCs and NSC-Ln229ev cells were significant ($P < 0.05$). Data are the means ± standard deviation (SD) of three experiments, Student's t –test. (B) Expression of Ki67 were detected in Ln229 cells, NSC-Ln229ev cells, and NSCs. Magnification 10×, Scale bars, 100 μm (A–I). Nuclei were stained with DAPI. (C) Ki67 positive cells of five fields for each cell line were numbered and compared. There were no significant differences between Ln229 and NSC-Ln229ev cells in Ki67 expression rates, the average percentage of Ki67 positive cells per field in NSCs decreased significantly. Data are the means ± SD of three experiments, Student's t –test, $^{***}P < 0.001$. (D) Clone formation was observed both in Ln229 and NSC-Ln229ev cells in soft agar assay, and there was no clone formation in NSCs. Magnification 20×, Scale bars, 100 μm (A–C). (E) All formed clones of five wells for each cell line were numbered and compared. The differences between Ln229 and NSC-Ln229ev cells in clone formation were significant. No clone was found in NSCs. Data are the means ± SD of three experiments, Student's t –test, $^{***}P < 0.001$.

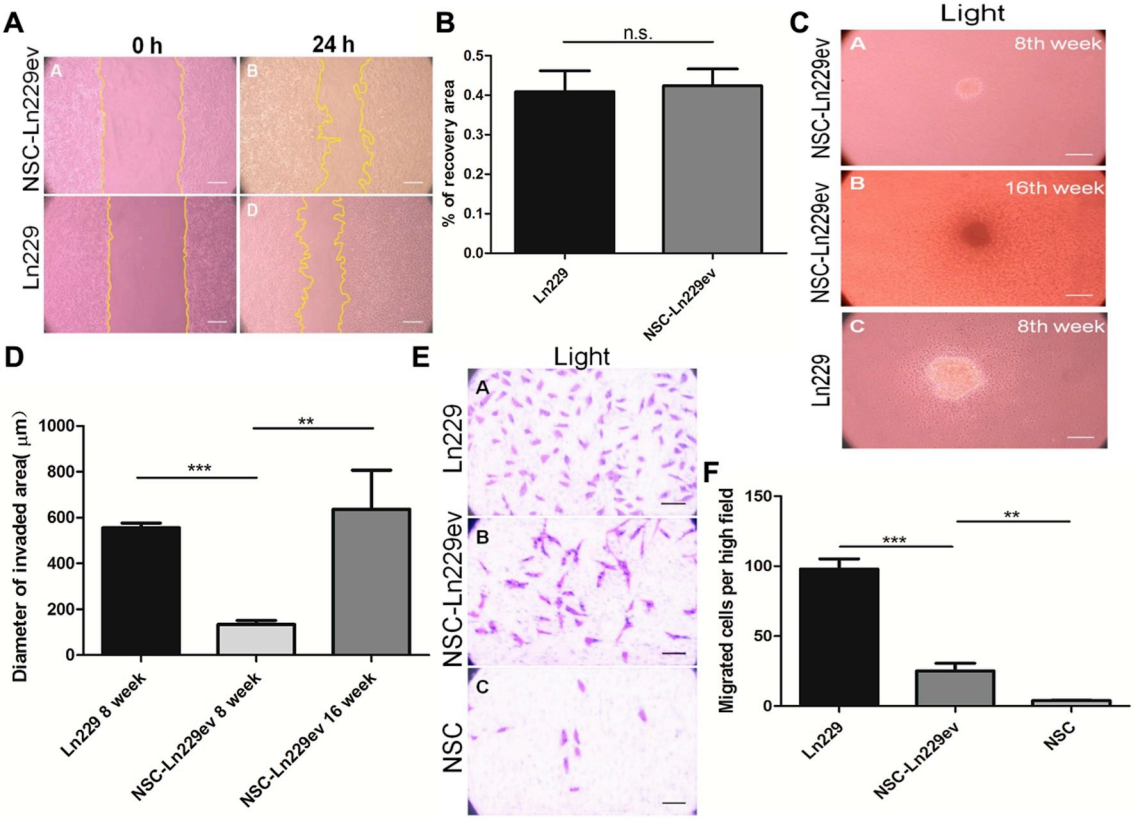

Fig. 4. Migration and invasion ability of NSC-Ln229ev cells. (A) In wound-healing assay, the wound areas recovered almost at the same rate both in Ln229 and NSC-Ln229ev cells during 24 h. Magnification 20×, Scale bars, 100 μm (A–D). (B) Wound-healing areas in five high-power fields for each cell line were calculated and compared. There were no significant differences between NSC-Ln229ev and Ln229 cells in terms of recovery percentage in wound-healing assays ($P > 0.05$). Data are the means ± SD of three experiments, Student's *t* –test. (C) In clone formation assays, NSC-Ln229ev cells formed clones were maintained for another 12 weeks, and the invaded areas increased obviously compared to the clones at 8th week, with clones of Ln229 cells as positive control. Magnification 20×, Scale bars, 100 μm (A–C). (D) Invaded areas of five clones formed by NSC-Ln229ev cells at 8th week and 16th week were calculated and compared. There were significant differences between these two groups in terms of invaded areas. The differences between Ln229 and NSC-Ln229ev cells in terms of invaded areas at 8th week were also significant. Data are the means ± SD of three experiments, Student's *t* –test, $^{***}P < 0.001$, $^{**}P < 0.01$. (E) A number of NSC-Ln229ev and Ln229 cells went through the matrigel treated membranes in transwell assays, and very few NSCs completed this, Magnification 20×, Scale bars, 100 μm (A–C). (F) Migrated cells of five high-power fields for each cell line were numbered and compared. There were significant differences between NSC-Ln229ev and NSCs in terms of average migrated cells per high-power field. Also there were significant differences between NSC-Ln229ev and Ln229 cells. Data are the means ± SD of three experiments, Student's *t* –test, $^{***}P < 0.001$, $^{**}P < 0.01$.

3.5. Enhancement of tumour-forming ability in nude mice by co-transplantation with NSC-Ln229ev and Ln229 cells

The tumour formation ability of NSC-Ln229ev cells in nude mice was examined, and no masses were observed in any of the NSC-Ln229ev-transplanted nude mice (see Supplementary Information Fig. S2). In contrast, the co-transplantation of NSC-Ln229ev and Ln229 cells resulted in an increase in tumour mass compared to that yielded from Ln229 cells alone, and the outcomes are displayed in Fig. 5A (A–H). Tumour sizes were measured and the differences in their volumes were statistically significant ($P < 0.001$, Fig. 5B). Histochemistry was then performed, and the results are displayed in Fig. 5C. The expression of GFAP, vimentin, and S100 confirmed the origin of these tumours. Further, there were no differences between the two groups in terms of the expression level of these three markers (Fig. 5D, $P > 0.05$). The average number of mitotic cells per high-power field in the co-transplant group was significantly higher than that with Ln229 cells alone (Fig. 5E, $P < 0.01$). Sox2 and Nestin, markers of stem cells, were positive in both groups (Fig. 5F). However, whereas there was no differences between the two groups in terms of the level of Nestin (Fig. 5D, $P > 0.05$), the average percentage of Sox2-positive cells in the co-transplant group was significantly higher than that in the group transplanted with Ln229 cells alone (Fig. 5G, $P < 0.001$); a similar pattern was also found for Ki67 expression (Fig. 5H, $P < 0.001$).

3.6. Single-cell sequencing reveals the heterogeneity of NSC-Ln229ev cells

As we found that NSC-Ln229ev cells were tumour-promoting or glioma-like cells, single-cell transcriptome sequencing was performed to uncover the details related to this transformation. NSC-Ln229ev cells were prepared for single-cell sequencing, with T0 cells and NSCs as positive and negative controls, respectively. Based on the transcriptome data set, NSC-Ln229ev cells were subdivided into clusters 0–8 using t-SNE analysis (Fig. 6A). Cell numbers for each cluster are displayed in Fig. 6B. Different clusters were classified by differentially expressed genes, and the results are shown by a heat-map (Fig. 6C). Each cluster had an exclusive pattern of gene expression, and the enriched biological processes associated with each cluster were identified by Gene Ontology analysis (Fig. 6C). For example, genes encoding proteins involved in cell cycle and DNA replication were highly expressed in cluster 3, whereas in cluster 1, most genes were mainly involved in the immune response. Similar results were obtained for T0 cells derived from a relapsed glioblastoma tumour, and 11 sub-clusters of T0 cells were obtained (see Supplementary information Table S1). Marker genes in each cluster were also found by the FindAllMarkers function in Seurat with default parameters. The expression maps of marker genes in each cluster from NSC-Ln229ev cells are shown in Fig. 6D.

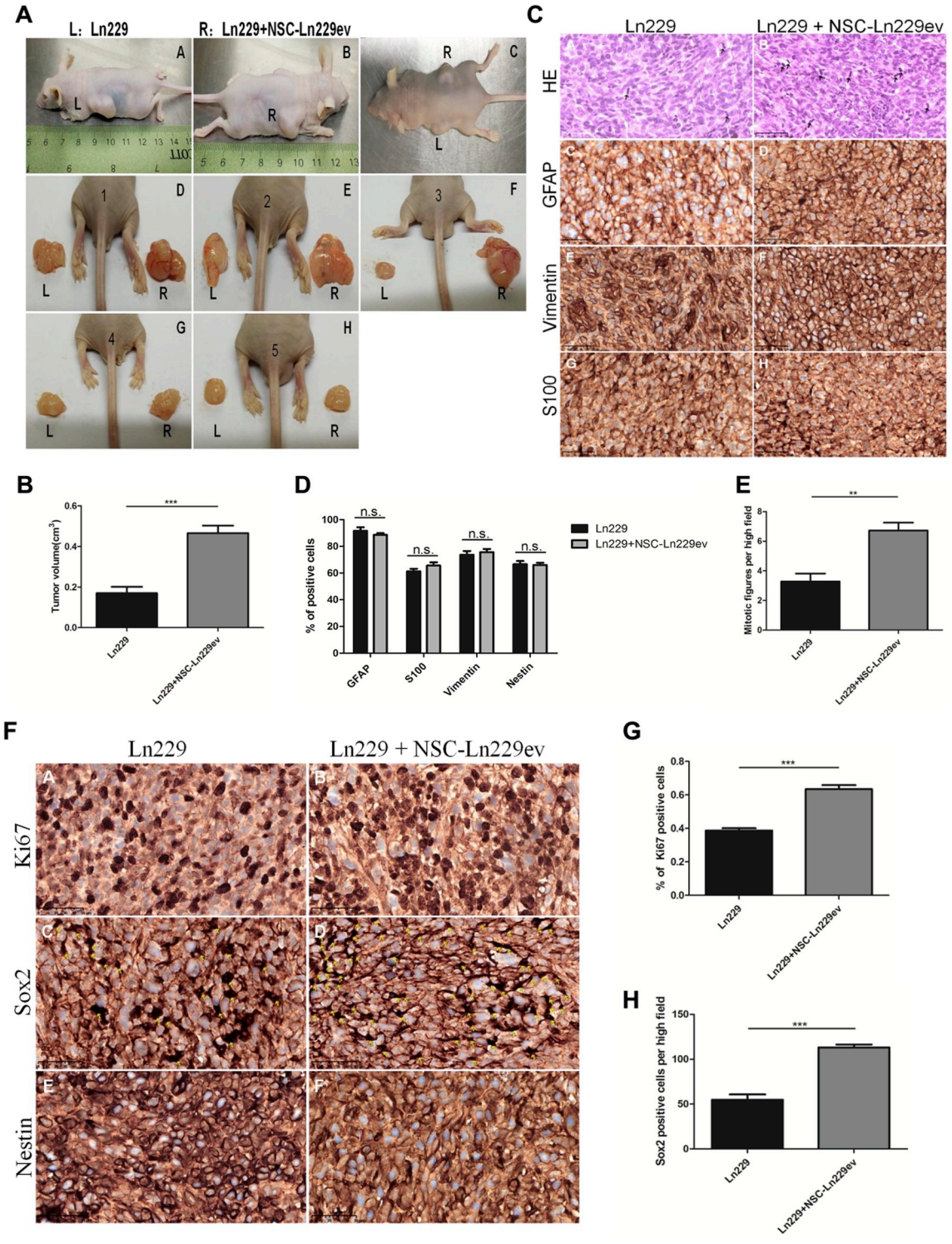

Fig. 5. Tumour formation ability was enhanced by co-transplantation in nude mice. (A) Ln229 cells together with NSC-Ln229ev cells or alone were injected into the right or left flanks of nude mice (n = 5), the tumour size in the right flanks of nude mice was larger than that in the left, as shown in A-H, L indicates left, R indicates right, 1–5 indicate five different mice. (B) Each tumour volume was calculated and compared, there were significant differences in terms of tumour volume between these two groups. Data are the means ± SD of three experiments, Student's *t* –test, ***$P < 0.001$. (C) HE staining and histochemistry were performed, mitotic figures were indicated in HE staining. The GFAP, S-100 and vimentin were all positive in both groups. Magnification 40×, Scale bars, 50 μm (A–H). (D) There were no differences between these two groups in expression level of Nestin, GFAP, S-100 and vimentin. Data are the means ± SD of three experiments, Student's *t* –test, $P > 0.05$. (E) Mitotic figures of five high-power fields were numbered in both groups and compared, and the differences were significant. Data are the means ± SD of three experiments, Student's *t* –test, **$P < 0.01$. (F) Ki67, Sox2 and Nestin were all positive in both groups. Magnification 40×, Scale bars, 50 μm (A–F). (G) Ki67 positive cells of five high-power fields in both groups were calculated and compared, there were significant differences between these two groups in terms of Ki67 expression rates. Data are the means ± SD of three experiments, Student's *t* –test, ***$P < 0.001$. (H) Sox2 positive cells of five high-power fields in both groups were numbered and compared, there were significant differences between these two groups in average Sox2 positive cells. Data are the means ± SD of three experiments, Student's *t* –test, ***$P < 0.001$.

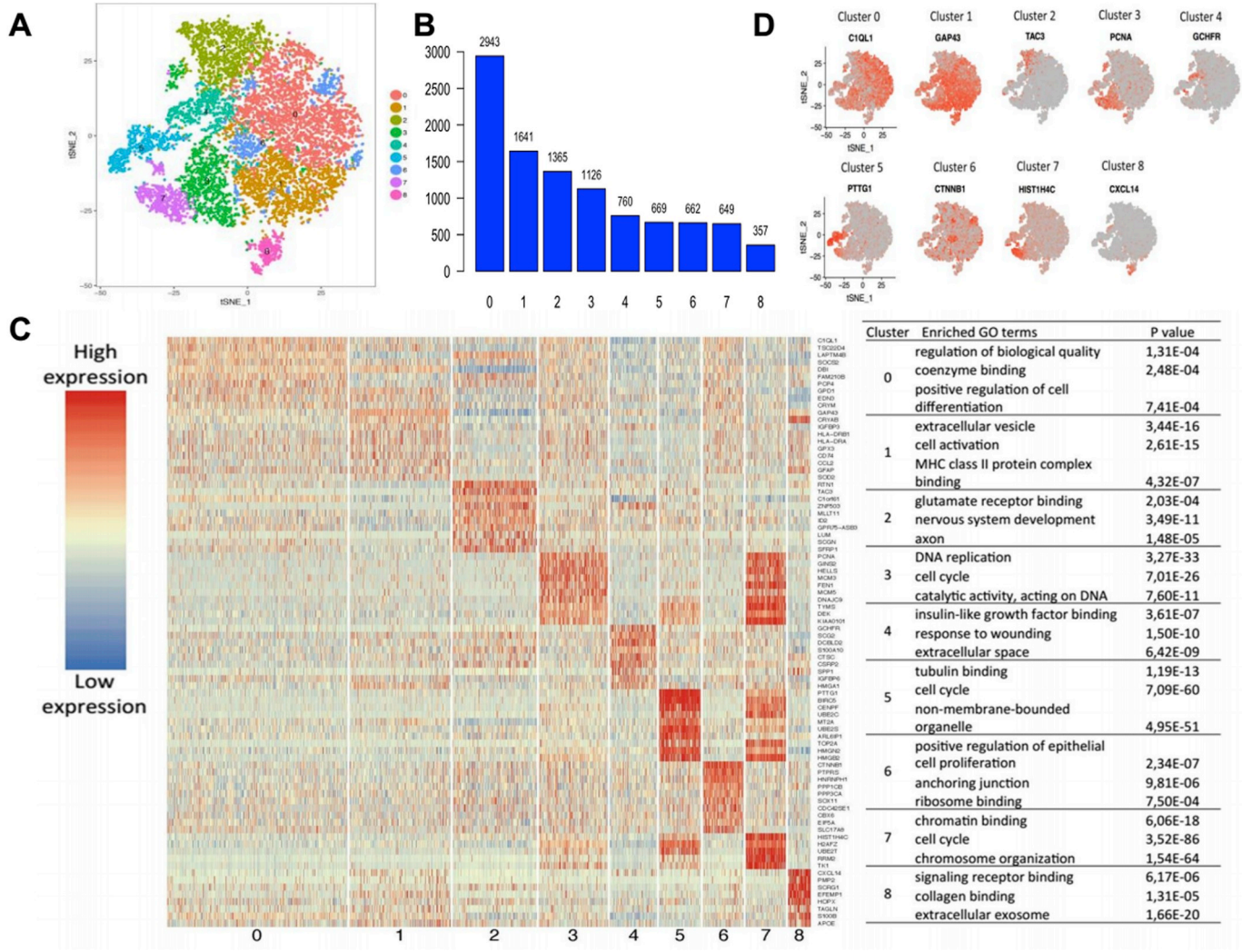

Cluster	Enriched GO terms	P value
0	regulation of biological quality	1,31E-04
	coenzyme binding	2,48E-04
	positive regulation of cell differentiation	7,41E-04
1	extracellular vesicle	3,44E-16
	cell activation	2,61E-15
	MHC class II protein complex binding	4,32E-07
2	glutamate receptor binding	2,03E-04
	nervous system development	3,49E-11
	axon	1,48E-05
3	DNA replication	3,27E-33
	cell cycle	7,01E-26
	catalytic activity, acting on DNA	7,60E-11
4	insulin-like growth factor binding	3,61E-07
	response to wounding	1,50E-10
	extracellular space	6,42E-09
5	tubulin binding	1,19E-13
	cell cycle	7,09E-60
	non-membrane-bounded organelle	4,95E-51
6	positive regulation of epithelial cell proliferation	2,34E-07
	anchoring junction	9,81E-06
	ribosome binding	7,50E-04
7	chromatin binding	6,06E-18
	cell cycle	3,52E-86
	chromosome organization	1,54E-64
8	signaling receptor binding	6,17E-06
	collagen binding	1,31E-05
	extracellular exosome	1,66E-20

Fig. 6. Single cell RNAseq analysis of NSC-Ln229ev cells. (A) Seurat clustering analysis identified nine sub-clusters (0–8) in NSC-Ln229ev cells shown in a t-SNE map, each dot represents one cell, and different colours denote different clusters. (B) Cell number for each cluster in NSC-Ln229ev cells were shown. (C) Top 10 differentially expressed genes for each cluster were shown in a heatmap, and the representative enriched items of Gene Oncology analysis for each cluster were displayed together. (D) Representative marker genes for each cluster were shown in t-SNE maps, each dot represents one cell, red colour indicates high expression.

3.7. Single-cell sequencing reveals a glioma-related cluster in NSC-Ln229ev cells

To determine which cluster from NSC-Ln229ev cells was more related to glioma, maker genes for each cluster were identified (see Supplementary information Table S2), and a gene panel comprising glioma-, CSC-, and NSC-related marker genes was established based on previous research (see Supplementary information Table S3) [23–28]. Genes in the panel were all searched in the marker gene list of clusters 0–8. Finally, cluster 8 was found to express more of these panel genes than any other cluster. Genes upregulated in gliomas and cancer stem cells were enriched in cluster 8. This result indicates that cluster 8 might be responsible for the malignancy of NSC-Ln229ev cells and could represent cancer stem cells. Weighted gene co-expression network analysis (WGCNA) was thus performed for cluster 8. *S100B*, *CXCL14*, *EFEMP1*, and *SCRG1* were identified in the core of the network (Fig. 7A). Further, the expression status of these four genes and several other glioma-related genes was explored, and results are displayed by a violin plot in Fig. 7B. *CXCL14*, *EFEMP1*, and *SCRG1* were almost exclusively expressed in cluster 8, and the expression levels of glioma-related genes *S100B*, *FABP7*, and *GFAP* were also much higher in cluster 8 than in other clusters. The expression status of *CXCL14*, *EFEMP1*, *SCRG1*, *S100B*, *FABP7*, and *GFAP* in NSCs was also explored (Fig. 7C). NSCs did not express *EFEMP1* and *GFAP*, in NSCs, and the levels of *CXCL14* and *SCRG1* in NSCs were similar in different clusters. These results indicate that *CXCL14*, *EFEMP1*, *SCRG1*, and *S100B* might be important for the transformation of NSCs into NSC-Ln229ev cells.

MELK and *VIM* are markers of NSCs [28], whereas *PTN* and *PTPRZ1* are indicators of cancer stem cells (CSCs) (Fig. 7B) [24]; almost all of these were highly expressed in cluster 8 NSC-Ln229ev cells. KEGG analyses were then performed to verify whether signalling pathways had been altered during the transformation of NSCs into NSC-Ln229ev cells. Genes from the peroxisome proliferator-activated receptor (PPAR) pathway were enriched in cluster 8 of NSC-Ln229ev cells based on KEGG analysis (Fig. 7D), whereas in NSCs, genes from the P53/MAPK/Toll-like receptor/NOD-like receptor signalling pathways were enriched (Fig. 7E). PPAR signalling is involved in inflammation, and oxidative stress, and plays a crucial role in a variety of cancers including glioblastoma, breast, pancreatic, leukaemia, and prostate tumours.

3.8. Joint t-SNE analysis reveals a unique cell cluster

To clarify the evolution of NSCs into NSC-Ln229ev cells, joint t-SNE analysis was performed with the transcriptome data set of NSCs and NSC-Ln229ev cells (Fig. 8A), and clusters 0–12 were identified. Cell numbers of each cluster are displayed in Fig. 8B. Interestingly, there

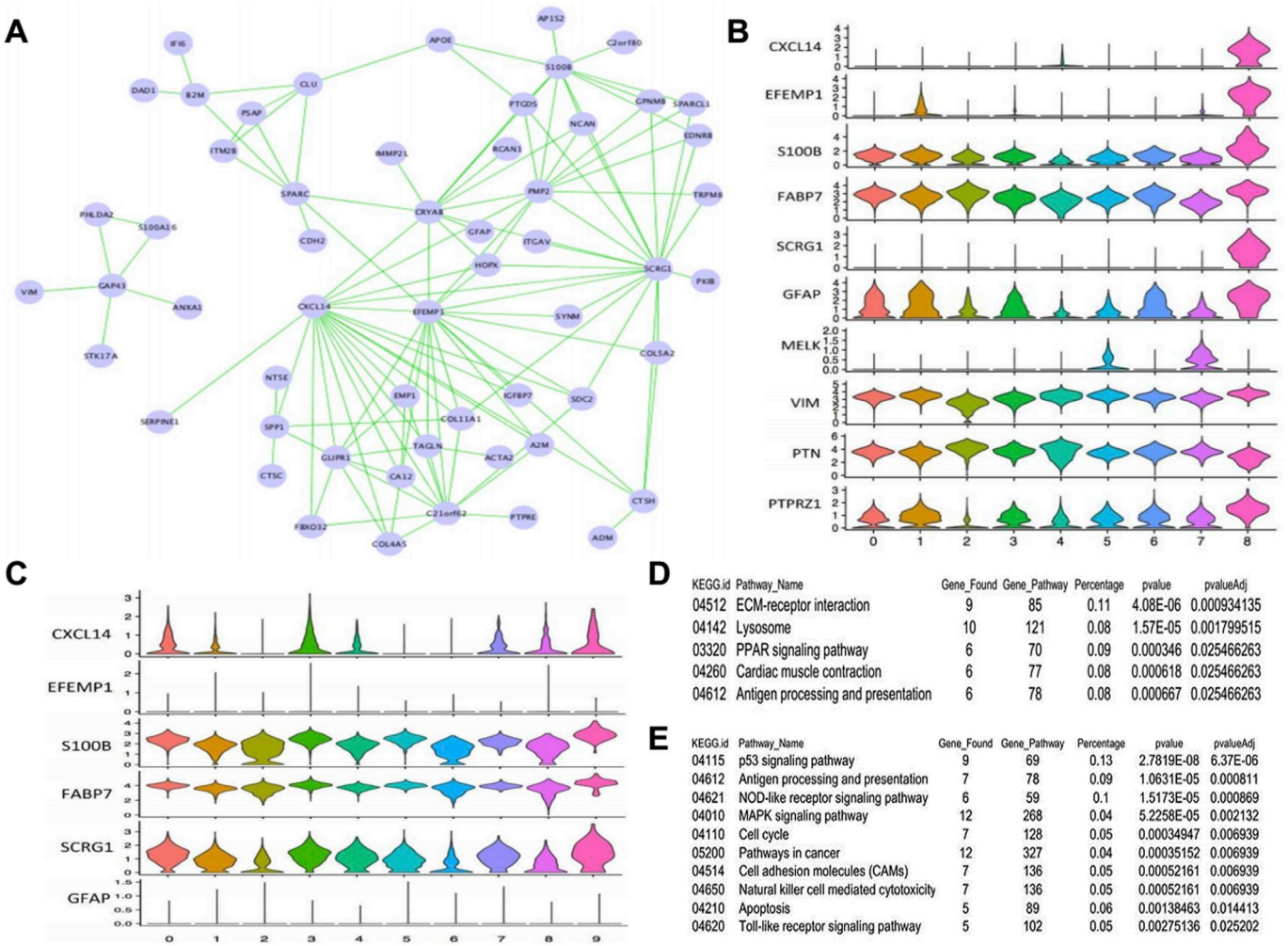

Fig. 7. Analysis of cluster 8 of NSC-Ln229ev cells. (A) WGCNA analysis of cluster 8 in NSC-Ln229ev cells were performed, and four genes were found at core of this gene co-expression network containing *CXCL14*, *EFEMP1*, *S100B*, and *SCRG1*. (B) Expression status of key genes for each cluster in NSC-Ln229ev cells were shown in a violin plot. Different colours denote different clusters. Y-axis indicates log-scaled expression level, X-axis indicates sub-clusters in NSC-Ln229ev cells. (C) Expression status of key genes for each cluster in NSCs were shown in a violin plot. Different colours denote different clusters. Y-axis indicates log-scaled expression level, X-axis indicates sub-clusters in NSC-Ln229ev cells. (D) Enriched signalling pathways were identified by KEGG analysis within cluster 8 of NSC-Ln229ev cells. (E) Enriched signalling pathways were identified by KEGG analysis within NSCs.

were only 62 NSC-Ln229ev cells in cluster 11, with no cells from NSCs; this result suggests that cluster 11 can best represent the transformation of NSCs into NSC-Ln229ev cells. Further exploration of cluster 11 revealed a list of marker genes with *GFAP*, *GLIPR1*, *CXCL14*, *EFEMP1*, *HMGA1*, and *CD44* included; the expression maps of several marker genes are depicted in Fig. 8C.

4. Discussion

EVs have been proven to play an important role in cell communication, particularly in the field of oncology [29]. A truncated and oncogenic form of the epidermal growth factor receptor (EGFRvIII), often expressed by gliomas, were transferred to EGFRvIII-negative cancer cells by microvesicles derived from glioma cells, leading to the activation of signalling pathways and transformation [30]. Meanwhile, mRNA, microRNA, and angiogenic proteins contained in microvesicles (exosomes) released by glioblastoma cells can be delivered to normal host cells, leading to tubule formation with endothelial cells; moreover, glioblastoma microvesicles are thought to stimulate the proliferation of human glioma cell lines [12]. Together, it has been concluded that EVs derived from gliomas are involved in tumour cell proliferation, invasion, malignancy, evasion of apoptosis, and resistance to immune and therapeutic agents [31].

Previous studies have been focused on the origin and molecular characteristics of glioblastomas for decades, and four subtypes have been classified based on the results of population sequencing analyses of hundreds of glioblastoma samples [25,32]. However, this is still relatively unclear. An integrated genomic analysis showed that glioblastoma exhibits extensive intra-tumour heterogeneity, with different subtypes incorporated into the same tumour and that clone evolution can be established within the tumour [33]. Therefore, there is a pressing need for new ways to determine the exact molecular characteristics of glioblastomas. Single-cell sequencing has been proven as a successful method to investigate comprehensive intra-tumour heterogeneity and tumour evolution [34,35], and we used this method to clarify the transformation of NSCs into tumour-promoting cells in this work.

In this research, an in vitro glioblastoma-relapse environment was mimicked by adding EVs derived from glioblastoma cell lines to the culture medium of NSCs. Changes in the expression pattern of neural cell markers indicated the differentiation of NSCs towards astrocytic and neurocytic cells, based on GFAP and NeuN, which are considered respective markers of these types. However, NSC-Ln229ev cells might still possess some properties unique to stem cells, as the stem cell markers Nestin and Sox2 were still positive. Other researchers have

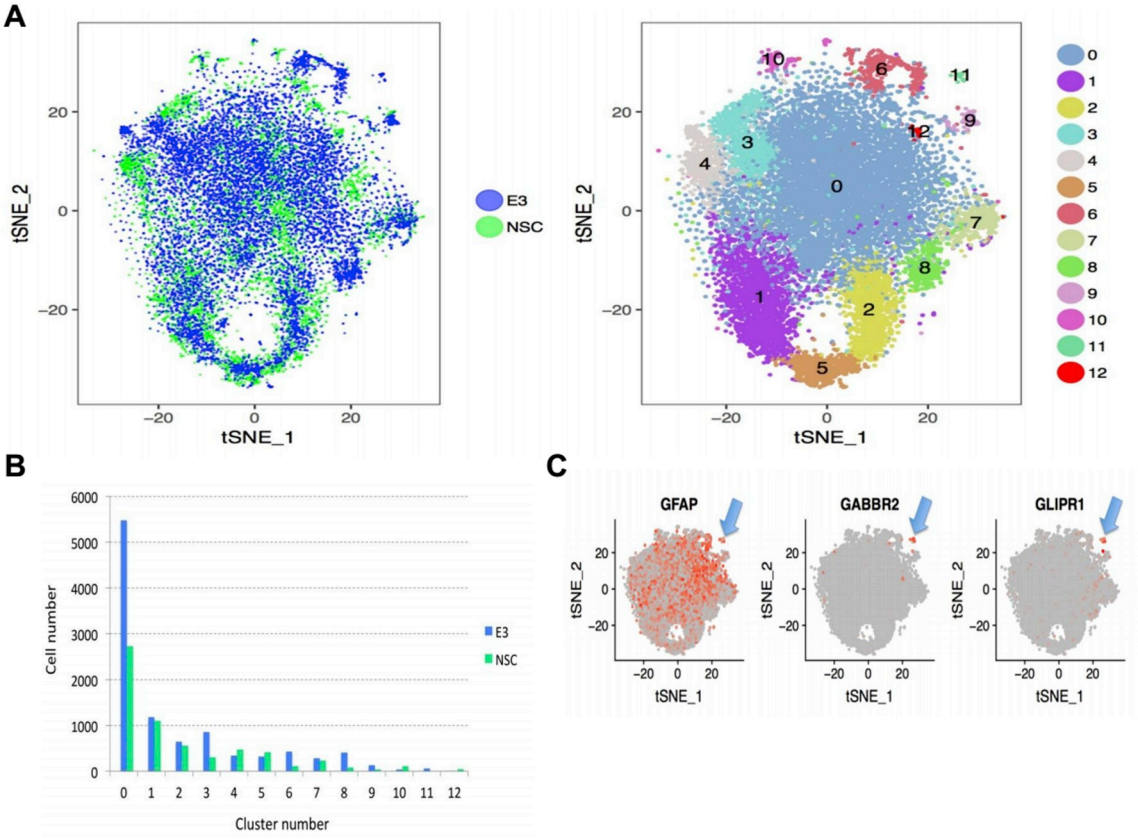

Fig. 8. Joint t-SNE analysis of NSCs and NSC-Ln229ev cells. (A) Joint t-SNE analysis identified thirteen sub-clusters (0-12) in NSC-Ln229ev cells and NSCs shown in a t-SNE map, blue colour denotes NSC-Ln229ev cells and green colour denotes NSCs (left), different colours denote different clusters (right). Each dot represents one cell. (B) Cell number for each cluster in NSC-Ln229ev cells and NSCs were displayed, blue colour denotes NSC-Ln229ev cells and green colour denotes NSCs. (C) Representative marker genes for cluster 11 in joint t-analysis of NSC-Ln229ev cells and NSCs were shown in t-SNE maps, each dot represents one cell, red colour indicates high expression. Blue arrow points to cluster 11.

found that transducing oncogenic lentiviral vectors into NSCs, astrocytes, and neurons in the brains of mice can give rise to gliomas with high stem cell marker expression [36]. Another study has also found that silencing SOX2 in glioblastoma tumour-initiating cells can halt cell proliferation, resulting in a loss of tumorigenicity [37]. Therefore, the positive expression of stem cell markers might be a characteristic of some glioma cells. In addition to changes in marker expression, NSCs differentiated into cells with enhanced capacity to proliferate, form clones, and migrate, and most importantly, these transformed cells were able to promote glioblastoma formation in vivo after co-transplantation with Ln229 cells. Together, these results proved that EVs from glioblastoma cells can transfer information to NSCs, resulting in the neoplastic transformation of the latter cell type in vitro. It has been reported that NSCs reside in SVZ areas [4], and recurrent glioblastomas are often found in white matter adjacent to these regions [5]. Therefore, NSCs probably participate in the recurrence of glioblastomas, during which malignant signals might be transferred by EVs. Furthermore, previous studies have found facts that human neural stem cells migrate towards intracranial glioma [38] or gliomas in vitro [39], and these cells distribute themselves extensively throughout the tumour bed and aggressively advance tumorigenesis [40]. Our results also indicate that NSC-Ln229ev cells can increase the proportion of cells with characteristics of cancer stem cells in xenografts, which could be the underlying reason as to why tumours in the co-transplanted group were much larger than those formed after the transplantation of Ln229 cells alone. NSC-Ln229ev cells alone were also subcutaneously transplanted into immunodeficient mice and failed to form tumours. There might be two causes for this. First, the in vivo GBM-relapsing environment was quite different from the conditions utilized in our experiments; second, NSC-Ln229ev cells alone might not be sufficient for tumour formation, and a particular microenvironment that consists of many types of tumour-associated cells could be required.

The transformed cells were further analysed by single-cell transcriptome sequencing to identify alterations at the transcriptional level, and the results demonstrated vast heterogeneity among the transformed glioma-like cells, as is the case for glioblastomas [33]. Cluster 8 of NSC-Ln229ev cells was identified as glioma CSCs based on the positive expression of an increased number of glioma-related genes, as compared to that in other clusters, such as *PTPRZ1*, *GFAP*, and *FABP7*. By WGCNA analysis, several key genes were found in cluster 8, including *S100B*, *CXCL14*, *EFEMP1*, and *SCRG1*, and these genes showed a specific expression pattern compared to that in other clusters based on a violin plot. Among these genes, *S100B* is a member of Ca^{2+}-binding protein family and is expressed in most gliomas; further, researchers have found that S100B promotes glioma growth via tumour-associated macrophages [41] and the suppression of S100B inhibits glioma growth [42]. *CXCL14* is a divergent member of the CXC chemokine family, which has a wide range of biological activities. It has been reported that gliomas attract microglia and polarize them into tumour-supporting cells by inducing several genes including *CXCL14* [43]. EFEMP1 was reported to bind epidermal growth factor receptor and activate downstream signalling pathways and another study discovered that miR-338–5p suppresses the proliferation, migration, and invasion of GBM cells by targeting EFEMP1 [44]. *SCRG1* is induced in transmissible spongiform encephalopathies and brain injuries and is associated with autophagy [45]. Another group discovered that SCRG1 participates in the self-renewal, differentiation, and migration of mesenchymal stem cells [46]. Our results suggest these genes might also play an important

role in the transformation of NSCs into glioma-like cells. Furthermore, results of joint t-SNE analysis of NSCs and NSC-Ln229ev cells identified a unique cluster, with 62 cells, exclusively from NSC-Ln229ev cells; thus the further exploration of these 62 cells could unveil the route of NSC transformation into NSC-Ln229ev cells. We also obtained a list of marker genes in this cluster containing *GFAP*, *GLIPR1*, *CXCL14*, *EFEMP1*, *HMGA1*, and *CD44*. It has been reported that *GLIPR1* is overexpressed in gliomas and regulates the growth, survival, and invasion of glioma cells [47]. Silencing *HMGA1* in glioblastoma stem cells can reduce stemness and temozolomide resistance [48]. Moreover, *CD44* is involved in glioma survival and migration [49]. Our results imply that these genes might also be important for the transformation of NSCs into NSC-Ln229ev cells.

Interestingly, a redirection of signalling pathways was also suggested to occur during EV-induced NSC transformation. PPARs, members of the steroid hormone receptor superfamily, are involved in energy metabolism, including PPARα, PPARβ/δ, and PPARγ. PPARα was reported to be abundant in glioblastoma and a potential therapeutic target for this disease. Researchers have also found that a PPARα antagonist results in the induction of cell death, an increase in radiosensitivity, and a decrease in migration among glioblastoma primary cells [50]. Interestingly, PPARγ is downregulated in gliomas and its activation inhibits various signalling cascades such as the JAK/STAT, WNT/β-catenin, and PI3K/Akt pathways, leading to reduced tumour growth, cell proliferation, and cell invasiveness [51]. Accordingly, whether glioma progresses might be dependent on the activation status of PPARα or PPARγ. Here, our results indicate that the activation of PPAR signalling might be involved in the transformation of NSCs into NSC-Ln229ev cells, and the PPAR pathway could thus be a potential therapeutic target for recurrent glioblastoma patients.

In conclusion, our results demonstrated the transformation of NSCs into tumour-promoting cells in vitro, which was induced by EVs derived from glioblastoma cells; we also suggest that this could be involved in glioblastoma relapse. During this transformation process, several key genes and possibly related signalling pathways were identified, which could represent novel therapeutic targets for recurrent glioblastomas. These results also imply a new strategy for treating glioblastoma patients, specifically the pre-processing of cells in the SVZ after surgical procedures to prevent or delay the disease recurrence.

Funding

This work was supported by National Natural Science Foundation of China [grant numbers 81272804, 81301066, 81672824]; the National Key Technology Research and Development Program [grant number 2014BAI04B02]; and the National High-tech R&D Program of China [grant number 863 Program, 2012AA020809].

Conflicts of interest

The authors declare that they have no competing interests.

Data availability

The accession number for sequencing data reported in this work is GEO: GSE136974. (The following secure token has been created to allow review of record GSE136974 while it remains in private status: cduzqqmqpjofhyh.)

CRediT authorship contribution statement

Jian Wang: Project administration, Data curation, Formal analysis. **Jialin Liu:** Project administration, Data curation, Formal analysis. **Guochen Sun:** Project administration, Data curation, Formal analysis. **Hengxing Meng:** Methodology. **Jiayin Wang:** Methodology. **Yunqian Guan:** Methodology. **Yiheng Yin:** Data curation. **Zhenyu Zhao:** Data curation. **Xiying Dong:** Data curation. **Shangjiong Yin:** Investigation. **Hongwei Li:** Methodology. **Yuefei Cheng:** Investigation. **Hao Wu:** Software. **Anhua Wu:** Conceptualization, Supervision, Funding acquisition. **Xinguang Yu:** Conceptualization, Supervision, Funding acquisition. **Ling Chen:** Conceptualization, Supervision, Funding acquisition.

Acknowledgments

The authors thank Lixian Wang (Technical Support Center, Tianjin Institute of Industrial Biotechnology, Chinese Academy of Science) for technical assistance in immunocytochemistry and transmission electron microscopy. The authors thank Elsevier Publisher for their assistance of language editing.

Appendix A. Supplementary data

Supplementary data to this article can be found online at https://doi.org/10.1016/j.canlet.2019.09.004.

References

[1] D.N. Louis, H. Ohgaki, O.D. Wiestler, W.K. Cavenee, P.C. Burger, A. Jouvet, et al., The 2007 WHO classification of tumours of the central nervous system, Acta Neuropathol. 114 (2007) 97–109.
[2] R. Stupp, W.P. Mason, M.J. van den Bent, M. Weller, B. Fisher, M.J.B. Taphoorn, et al., Radiotherapy plus concomitant and adjuvant temozolomide for glioblastoma, N. Engl. J. Med. 352 (2005) 987–996.
[3] R. Stupp, M.E. Hegi, W.P. Mason, M.J. van den Bent, M.J.B. Taphoorn, R.C. Janzer, et al., Effects of radiotherapy with concomitant and adjuvant temozolomide versus radiotherapy alone on survival in glioblastoma in a randomised phase III study: 5-year analysis of the EORTC-NCIC trial, Lancet Oncol. 10 (2009) 459–466.
[4] C.B. Johansson, S. Momma, D.L. Clarke, M. Risling, U. Lendahl, J. Frisen, Identification of a neural stem cell in the adult mammalian central nervous system, Cell 96 (1999) 25–34.
[5] B.M. Ellingson, A. Lai, R.J. Harris, J.M. Selfridge, W.H. Yong, K. Das, et al., Probabilistic radiographic atlas of glioblastoma phenotypes, AJNR. Am. J. Neuroradiol. 34 (2013) 533–540.
[6] N.A. Charles, E.C. Holland, R. Gilbertson, R. Glass, H. Kettenmann, The brain tumor microenvironment, Glia 59 (2011) 1169–1180.
[7] S. Atay, S. Banskota, J. Crow, G. Sethi, L. Rink, A.K. Godwin, Oncogenic KIT-containing exosomes increase gastrointestinal stromal tumor cell invasion, Proc. Natl. Acad. Sci. U.S.A. 111 (2014) 711–716.
[8] H. Valadi, K. Ekstrom, A. Bossios, M. Sjostrand, J.J. Lee, J.O. Lotvall, Exosome-mediated transfer of mRNAs and microRNAs is a novel mechanism of genetic exchange between cells, Nat. Cell Biol. 9 (2007) 654–672.
[9] A. Hoshino, B. Costa-Silva, T.L. Shen, G. Rodrigues, A. Hashimoto, M.T. Mark, et al., Tumour exosome integrins determine organotropic metastasis, Nature 527 (2015) 329–335.
[10] T. Umezu, H. Tadokoro, K. Azuma, S. Yoshizawa, K. Ohyashiki, J.H. Ohyashiki, Exosomal miR-135b shed from hypoxic multiple myeloma cells enhances angiogenesis by targeting factor-inhibiting HIF-1, Blood 124 (2014) 3748–3757.
[11] T.L. Whiteside, Tumor-derived exosomes and their role in cancer progression, Adv. Clin. Chem. 74 (2016) 103–141.
[12] J. Skog, T. Wuerdinger, S. van Rijn, D.H. Meijer, L. Gainche, M. Sena-Esteves, et al., Glioblastoma microvesicles transport RNA and proteins that promote tumour growth and provide diagnostic biomarkers, Nat, Cell Biol. 10 (2008) 1470–1479.
[13] M. Katakowski, B. Buller, X.G. Zheng, Y. Lu, T. Rogers, O. Osobamiro, et al., Exosomes from marrow stromal cells expressing miR-146b inhibit glioma growth, Cancer Lett. 335 (2013) 201–204.
[14] P. Kucharzewska, H.C. Christianson, J.E. Welch, K.J. Svensson, E. Fredlund, M. Ringner, et al., Exosomes reflect the hypoxic status of glioma cells and mediate hypoxia-dependent activation of vascular cells during tumor development, Proc. Natl. Acad. Sci. U.S.A. 110 (2013) 7312–7317.
[15] A. Bronisz, Y. Wang, M.O. Nowicki, P. Peruzzi, K.I. Ansari, D. Ogawa, et al., Extracellular vesicles modulate the glioblastoma microenvironment via a tumor suppression signaling network directed by miR-1, Cancer Res. 74 (2014) 738–750.
[16] L. Manterola, E. Guruceaga, J. Gallego Perez-Larraya, M. Gonzalez-Huarriz, P. Jauregui, S. Tejada, et al., A small noncoding RNA signature found in exosomes of GBM patient serum as a diagnostic tool, Neuro Oncol. 16 (2014) 520–527.
[17] D.R. Santiago-Dieppa, J. Steinberg, D. Gonda, V.J. Cheung, B.S. Carter, C.C. Chen, Extracellular vesicles as a platform for 'liquid biopsy' in glioblastoma patients, Expert Rev. Mol. Diagn. 14 (2014) 819–825.
[18] J. Gourlay, A.P. Morokoff, R.B. Luwor, H.J. Zhu, A.H. Kaye, S.S. Stylli, The emergent role of exosomes in glioma, J. Clin. Neurosci. 35 (2017) 13–23.
[19] F. Tang, C. Barbacioru, Y. Wang, E. Nordman, C. Lee, N. Xu, et al., mRNA-Seq whole-transcriptome analysis of a single cell, Nat. Methods 6 (2009) 377–382.
[20] E. Shapiro, T. Biezuner, S. Linnarsson, Single-cell sequencing-based technologies will revolutionize whole-organism science, Nat. Rev. Genet. 14 (2013) 618–630.
[21] F. Buettner, K.N. Natarajan, F.P. Casale, V. Proserpio, A. Scialdone, F.J. Theis, et al.,

Computational analysis of cell-to-cell heterogeneity in single-cell RNA-sequencing data reveals hidden subpopulations of cells, Nat. Biotechnol. 33 (2015) 155–160.
[22] Y. Guan, X. Li, H. Zou, X. Yan, C. Zhao, J. Wang, et al., Multiparameter characterization confirms apoptosis as the primary cause of reduced self-renewal capacity in cultured human fetal neural stem cells, Cell. Physiol. Biochem. 38 (2016) 2123–2138.
[23] C.M. Zhao, W. Deng, F.H. Gage, Mechanisms and functional implications of adult neurogenesis, Cell 132 (2008) 645–660.
[24] Y. Shi, Y.F. Ping, W. Zhou, Z.C. He, C. Chen, B.S. Bian, et al., Tumour-associated macrophages secrete pleiotrophin to promote PTPRZ1 signalling in glioblastoma stem cells for tumour growth, Nat. Commun. 8 (2017) 15080–15086.
[25] L. Chin, M. Meyerson, K. Aldape, D. Bigner, T. Mikkelsen, S. VandenBerg, et al., Comprehensive genomic characterization defines human glioblastoma genes and core pathways, Nature 455 (2008) 1061–1068.
[26] C.W. Brennan, R.G.W. Verhaak, A. McKenna, B. Campos, H. Noushmehr, S.R. Salama, et al., The somatic genomic landscape of glioblastoma, Cell 155 (2013) 462–477.
[27] H. Ohgaki, P. Kleihues, Genetic pathways to primary and secondary glioblastoma, Am. J. Pathol. 170 (2007) 1445–1453.
[28] H.S. Phillips, S. Kharbanda, R.H. Chen, W.F. Forrest, R.H. Soriano, T.D. Wu, et al., Molecular subclasses of high-grade glioma predict prognosis, delineate a pattern of disease progression, and resemble stages in neurogenesis, Cancer Cell 9 (2006) 157–173.
[29] M. Tkach, C. Thery, Communication by extracellular vesicles: where we are and where we need to go, Cell 164 (2016) 1226–1232.
[30] K. Al-Nedawi, B. Meehan, J. Micallef, V. Lhotak, L. May, A. Guha, et al., Intercellular transfer of the oncogenic receptor EGFrvIII by microvesicles derived from tumour cells, Nat, Cell Biol. 10 (2008) 619–624.
[31] D.A. Chistiakov, V.P. Chekhonin, Extracellular vesicles shed by glioma cells: pathogenic role and clinical value, Tumor Biol. 35 (2014) 8425–8438.
[32] R.G. Verhaak, K.A. Hoadley, E. Purdom, V. Wang, Y. Qi, M.D. Wilkerson, et al., Integrated genomic analysis identifies clinically relevant subtypes of glioblastoma characterized by abnormalities in PDGFRA, IDH1, EGFR, and NF1, Cancer Cell 17 (2010) 98–110.
[33] A. Sottoriva, I. Spiteri, S.G.M. Piccirillo, A. Touloumis, V.P. Collins, J.C. Marioni, et al., Intratumor heterogeneity in human glioblastoma reflects cancer evolutionary dynamics, Proc. Natl. Acad. Sci. U.S.A. 110 (2013) 4009–4014.
[34] N. Navin, J. Kendall, J. Troge, P. Andrews, L. Rodgers, J. McIndoo, et al., Tumour evolution inferred by single-cell sequencing, Nature 472 (2011) 90–119.
[35] M. Meyer, J. Reimand, X. Lan, R. Head, X. Zhu, M. Kushida, et al., Single cell-derived clonal analysis of human glioblastoma links functional and genomic heterogeneity, Proc. Natl. Acad. Sci. U.S.A. 112 (2015) 851–856.
[36] D. Friedmann-Morvinski, E.A. Bushong, E. Ke, Y. Soda, T. Marumoto, O. Singer, et al., Dedifferentiation of neurons and astrocytes by oncogenes can induce gliomas in mice, Science 338 (2012) 1080–1084.
[37] R.M.R. Gangemi, F. Griffero, D. Marubbi, M. Perera, M.C. Capra, P. Malatesta, et al., SOX2 silencing in glioblastoma tumor-initiating cells causes stop of proliferation and loss of tumorigenicity, Stem Cells 27 (2009) 40–48.
[38] J.Y. Jeon, J.H. An, S.U. Kim, H.G. Park, M.A. Lee, Migration of human neural stem cells toward an intracranial glioma, Exp. Mol. Med. 40 (2008) 84–91.
[39] O. Heese, A. Disko, D. Zirkel, M. Westphal, K. Lamszus, Neural stem cells migration toward gliomas in vitro, Neuro Oncol. 7 (2005) 476–484.
[40] K.S. Aboody, A. Brown, N.G. Rainov, K.A. Bower, S. Liu, W. Yang, et al., Neural stem cells display extensive tropism for pathology in adult brain: evidence from intracranial gliomas, Proc. Natl. Acad. Sci. U.S.A. 97 (2000) 12846–12851.
[41] H. Wang, L. Zhang, I.Y. Zhang, X. Chen, A. Da Fonseca, S. Wu, H. Ren, et al., S100B promotes glioma growth through chemoattraction of myeloid-derived macrophages, Clin. Cancer Res. 19 (2013) 3764–3775.
[42] H. Gao, I.Y. Zhang, L. Zhang, Y. Song, S. Liu, H. Ren, et al., S100B suppression alters polarization of infiltrating myeloid-derived cells in gliomas and inhibits tumor growth, Cancer Lett. 439 (2018) 91–100.
[43] A. Ellert-Miklaszewska, M. Dabrowski, M. Lipko, M. Sliwa, M. Maleszewska, B. Kaminska, Molecular definition of the pro-tumorigenic phenotype of glioma-activated microglia, Glia 61 (2013) 1178–1190.
[44] D. Lei, F. Zhang, D. Yao, N. Xiong, X. Jiang, H. Zhao, MiR-338-5p suppresses proliferation, migration, invasion, and promote apoptosis of glioblastoma cells by directly targeting EFEMP1, Biomed. Pharmacother. 89 (2017) 957–965.
[45] M. Dron, Y. Bailly, V. Beringue, A.M. Haeberle, B. Griffond, P.Y. Risold, et al., Scrg1 is induced in TSE and brain injuries, and associated with autophagy, Eur. J. Neurosci. 22 (2005) 133–146.
[46] E. Aomatsu, N. Takahashi, S. Sawada, N. Okubo, T. Hasegawa, M. Taira, et al., Novel SCRG1/BST1 axis regulates self-renewal, migration, and osteogenic differentiation potential in mesenchymal stem cells, Sci. Rep. 4 (2014) 3652–3660.
[47] T. Rosenzweig, A. Ziv-Av, C. Xiang, W. Lu, S. Cazacu, D. Taler, et al., Related to testes-specific, vespid, and pathogenesis protein-1 (RTVP-1) is overexpressed in gliomas and regulates the growth, survival, and invasion of glioma cells, Cancer Res. 66 (2006) 4139–4148.
[48] M. Colamaio, N. Tosti, F. Puca, A. Mari, R. Gattordo, Y. Kuzay, et al., HMGA1 silencing reduces stemness and temozolomide resistance in glioblastoma stem cells, Expert Opin. Ther. Targets 20 (2016) 1169–1179.
[49] R.L. Klank, S.A. Decker Grunke, B.L. Bangasser, C.L. Forster, M.A. Price, T.J. Odde, et al., Biphasic dependence of glioma survival and cell migration on CD44 expression level, Cell Rep. 18 (2017) 23–31.
[50] E. Benedetti, M. d'Angelo, A. Ammazzalorso, G.L. Gravina, C. Laezza, A. Antonosante, et al., PPARalpha antagonist AA452 triggers metabolic Reprogramming and increases sensitivity to Radiation therapy in human glioblastoma primary cells, J. Cell. Physiol. 232 (2017) 1458–1466.
[51] A. Vallee, Y. Lecarpentier, R. Guillevin, J.N. Vallee, Opposite interplay between the canonical WNT/beta-catenin pathway and PPAR gamma: a potential therapeutic target in gliomas, Neurosci. Bull 34 (2018) 573–588.